Ryanodine Receptor Regulation by Intramolecular Interaction between Cytoplasmic and Transmembrane Domains

Christopher H. George,*† Hala Jundi,* N. Lowri Thomas,* Mark Scoote,‡ Nicola Walters,* Alan J. Williams,‡ and F. Anthony Lai*

*Wales Heart Research Institute, Department of Cardiology, University of Wales College of Medicine, Cardiff, United Kingdom CF14 4XN; and ‡National Heart and Lung Institute, Imperial College of Science Technology and Medicine, London, United Kingdom SW3 6LY

Ryanodine receptors (RyR) function as Ca^{2+} channels that regulate Ca^{2+} release from intracellular stores to control a diverse array of cellular processes. The massive cytoplasmic domain of RyR is believed to be responsible for regulating channel function. We investigated interaction between the transmembrane Ca^{2+}-releasing pore and a panel of cytoplasmic domains of the human cardiac RyR in living cells. Expression of eGFP-tagged RyR constructs encoding distinct transmembrane topological models profoundly altered intracellular Ca^{2+} handling and was refractory to modulation by ryanodine, FKBP12.6 and caffeine. The impact of coexpressing dsRed-tagged cytoplasmic domains of RyR2 on intracellular Ca^{2+} phenotype was assessed using confocal microscopy coupled with parallel determination of in situ protein: protein interaction using fluorescence resonance energy transfer (FRET). Dynamic interactions between RyR cytoplasmic and transmembrane domains were mediated by amino acids 3722–4610 (Interacting or "I"-domain) which critically modulated intracellular Ca^{2+} handling and restored RyR sensitivity to caffeine activation. These results provide compelling evidence that specific interaction between cytoplasmic and transmembrane domains is an important mechanism in the intrinsic modulation of RyR Ca^{2+} release channels.

INTRODUCTION

Ryanodine receptors are large tetrameric channels that coordinate Ca^{2+} release from the sarco/endoplasmic reticulum to directly regulate Ca^{2+}-dependent cellular processes (Berridge *et al.*, 2000; Carafoli, 2002; Fill and Copello, 2002). Modulation of RyR Ca^{2+} release activity is achieved by the concerted actions of numerous intracellular effectors including localized $[Ca^{2+}]$, phosphorylation and nitrosylation, cellular redox status, and the intrinsic organization of RyR into arrays (Meissner, 1994; Eu *et al.*, 2000; Yin and Lai, 2000; Sun *et al.*, 2001; Williams *et al.*, 2001). The transmembrane carboxyl-terminal (C-terminus) ~1000 aa of RyR constitutes the Ca^{2+}-releasing pore (Bhat *et al.*, 1997; Xu *et al.*, 2000) and contains the site of ryanodine binding (Callaway *et al.*, 1994; Witcher *et al.*, 1994), multiple interactive Ca^{2+} inactivation sites (Du and MacLennan, 1999) and is critical for tetrameric oligomerization of the intact RyR channel (Gao *et al.*, 1997; Stewart *et al.*, 2003). Aberrant regulation of the RyR Ca^{2+}-releasing pore is pathogenic and is implicated in heart failure, malignant hyperthermia (MH), and stress-induced ventricular tachycardia (Marx *et al.*, 2000; McCarthy *et al.*, 2000; George *et al.*, 2003a). The amino (N)-terminus of RyR, which contains numerous modular regulatory domains (Williams *et al.*, 2001), is proposed to interact with the Ca^{2+} pore to modulate Ca^{2+} release through the intact RyR channel pore

in vitro (Ikemoto and Yamamoto, 2000), and defective intra-RyR interactions are likely to be causative of aberrant Ca^{2+} release in RyR-linked pathology (Zorzato *et al.*, 1996; El-Hayek *et al.*, 1999; Yamamoto *et al.*, 2000; Yamamoto and Ikemoto, 2002). Activation of the RyR channel is associated with conformational reorganization of the cytoplasmic N-terminal catalytic structure and rotation of the C-terminal transmembrane assembly (El-Hayek *et al.*, 1995; Orlova *et al.*, 1996; Sharma *et al.*, 2000).

The precise topology of the transmembrane (TM) region within the RyR C-terminus also remains to be fully defined with models predicting 4, 6, and 10 TM-spanning segments (Takeshima *et al.*, 1989; Zorzato *et al.*, 1990; Tunwell *et al.*, 1996; Du *et al.*, 2002). Although cryo-EM studies demonstrated that the TM domain could physically accommodate 10 membrane-spanning domains (Orlova *et al.*, 1996; Sharma *et al.*, 2000), complementary strategies predicted that the C-terminus of each RyR subunit contains four or six TM-spanning regions (Callaway *et al.*, 1994; Witcher *et al.*, 1994; Grunwald and Meissner, 1995; Bhat *et al.*, 1997; Du *et al.*, 2002). The four-TM model is further supported by the finding that TM9 (Zorzato *et al.*, 1990)/TM5 (Tunwell *et al.*, 1996) forms part of the ion conduction pore (P-loop) analogous to that identified in *Streptomyces lividans* K^+ channel (Doyle *et al.*, 1998) and is therefore not membrane spanning (Balshaw *et al.*, 1999). Consequently, to preserve the cytoplasmic orientation of the RyR N- and extreme C-termini (~100 aa), TM3 (Tunwell *et al.*, 1996)/TM7 (Zorzato *et al.*, 1990) is unlikely to be a bona fide membrane-spanning domain on the basis of its relatively low hydrophobicity and lack of homology with other Ca^{2+}-releasing channels (Williams *et*

al., 2001; Du *et al.*, 2002). This revised model of transmembrane assembly is supported by biophysical characterization of the RyR conduction pore, which demonstrated a voltage drop nearer the lumenal side of the membrane, consistent with the existence of a P-loop structure (Tinker and Williams, 1995) and that mutagenesis of the putative RyR selectivity filter (GGIGD motif) significantly altered single-channel conductance, ionic selectivity, caffeine sensitivity, and ryanodine binding (Zhao *et al.*, 1999; Gao *et al.*, 2000; Du *et al.*, 2001; Chen *et al.*, 2002).

We therefore postulated that residues ~3900–4450 (TM1–4; Zorzato *et al.*, 1990) in the human cardiac RyR do not form TM domains, but rather that they represent regions of hydrophobicity that facilitate the spatial organization of the N- and C-terminal domains in the intact channel and permit the transduction of complex cytoplasmic modulatory events to the Ca^{2+} channel pore. To investigate this hypothesis, we inducibly expressed eGFP-tagged RyR2 fragments corresponding to the putative 4TM and 10TM arrangements (aa 4485–4967 and aa 3722–4967, respectively) in combination with dsRed-tagged RyR2 cytoplasmic (N-terminal) domains to more precisely determine, 1) the modulatory interactions that occurred between the N- and C-terminal domains and 2) the effect of such interactions on Ca^{2+} homeostasis in a cellular context. IntraRyR interactions occur below the limit of resolution of light microscopy, and we used fluorescence resonance energy transfer (FRET; Day *et al.*, 2001; Kenworthy, 2001; Truong and Ikura, 2001) between the eGFP and dsRed fusion partners to monitor the association between these domains. Our results provide direct evidence for functional coupling between disparate regions of the RyR mediated by an interacting domain ("I"-domain; 3722–4610 amino acids) that plays a pivotal regulatory role in Ca^{2+} channel function.

MATERIALS AND METHODS

Construction of TM and Cytoplasmic RyR2 Domains

A cDNA fragment of human RyR2 (Tunwell *et al.*, 1996) encoding the open reading frames (ORF) of 13574–15023 bp (aa 4485–4967; RyR2[4TM]) was generated by PCR amplification using *Pfu* polymerase and oligonucleotides (5′ cccgccgccaccatggcatatcaacagaaactt 3′/5′ cagcatttagctggtcttcatactgtt 3′). A *Hin*dIII/*Xho*I (11288–15335 bp) fragment of RyR2 encoding amino acids 3722–4967 (RyR2[10TM]) was excised. RyR2 cassettes were inserted in-frame at the carboxyl-terminus of enhanced green fluorescent protein (eGFP) in peGFP-C3 (CLONTECH, Palo Alto, CA) and eGFP-tagged RyR2[4TM] and RyR2[10TM] were subsequently transferred into pIND (Invitrogen, Carlsbad, CA) at *Nhe*I/ *Bam*HI restriction sites. Although we have named the longer recombinant fragment RyR2[10TM] because it was originally proposed to encode 10 TM domains (Zorzato *et al.*, 1990) and refer to it as such throughout this study, it should be noted that this construct may encode the four or six TM arrangements (Takeshima *et al.*, 1989; Tunwell *et al.*, 1996; Du *et al.*, 2002). Similarly, RyR2[4TM] may also encode six TM domains (Tunwell *et al.*, 1996).

A *Spe*I/*Nhe*I fragment of RyR2 (−12–10015 bp) encoding amino acids 1–3298 was inserted in frame at the 5′ terminus of the red fluorescent protein from *Discosoma* (dsRed; Matz *et al.*, 1999) in pdsRed-N1 (CLONTECH) to generate p3298[Red]. A *Nhe*I-*Hin*dIII fragment (10015–11288 bp; 3298–3722 aa) was ligated into pdsRed followed by subsequent insertion of the *Spe*I/*Nhe*I fragment (1–3298 aa) to create p3722[Red]. To generate p4353[Red] and p4610[Red], we constructed an intermediate (pInt[Red]) by amplifying 10015–12088 using oligonucleotides (5′ gaagaggctagcagtgtttcccagcctat 3′/5′ attaccctcgagcatggacagcaacatgc 3′ containing *Nhe*I and *Xho*I restriction sites, respectively). The introduction of an *Xho*I site (ctcgag vs. ttagaa in wild-type human RyR) retained the amino acid code (Leu-Glu). The 2.07-kb fragment was digested with *Nhe*I/*Xho*I and ligated into p3298[Red] to create pInt[Red]. cDNA fragments corresponding to 12072–13193 and 12072–13948 bp were amplified from full-length RyR2 using oligonucleotides containing *Xho*I linkers and were ligated into pInt[Red] to create p4353[Red] or p4610[Red], respectively. All plasmid propagation was done in *Escherichia coli* XL-10Gold (Stratagene, La Jolla, CA) as described previously (George *et al.*, 2003c) and constructs were verified by automated sequencing (ABI3100; Applied Biosystems, Foster City, CA).

Expression of RyR2 TM and Cytoplasmic Domains

Stable populations of CHO cells transfected with pVgRxR (Invitrogen; CHO[RxR]) were selected and maintained in complete Ham's F-12 medium (George *et al.*, 2003c) containing zeocin (500 μg/ml). Postselection, CHO[RxR] cells stably expressing RyR2 C-termini were further selected using G418 sulfate (500 μg/ml). The expression levels and intracellular targeting of RyR2[4TM] and RyR2[10TM] in clonally derived cell populations (>60 clones) were determined after induction with ponasterone A (ponA; 5 μM, 24 h; No *et al.*, 1996). Cell clones exhibiting the highest induction of RyR2[4TM] (clone G7) or RyR2[10TM] (clone E6) were isolated and used throughout this study.

CHO[RxR], G7, or E6 were transfected with 3298[Red], 3722[Red], 4353[Red], or 4610[Red] using Lipofectamine 2000 (Invitrogen). After transfection with RyR2 N-terminal domains (36–48 h posttransfection), expression of RyR2[4TM] or RyR2[10TM] in G7 or E6, respectively, was induced using ponA (5 μM, 24 h). Experiments were performed on cells ~72 h after the transfection of dsRed-tagged RyR2 N-termini, which appeared to maximize the green-to-red maturation of the dsRed fluorophore (Baird *et al.*, 2000).

The induction profile of recombinant protein expression in G7 and E6 cell lines was determined after addition of ponA (0–20 μM) for 24 h. Microsomal, nuclear, and cytoplasmic fractions were prepared and immunoblotted as described previously using anti-RyR2 antibodies pAb129 (epitope: RyR2 aa 4674–4697) or pAb2143 (epitope: RyR2 aa 91–105) followed by detection using donkey anti-rabbit antibody conjugated to horseradish peroxidase (Santa Cruz Biotechnology, Santa Cruz, CA) and chemiluminescence reagents (Supersignal, Pierce, Rockford, IL; George *et al.*, 2003c). To determine the subcellular localization of recombinant protein in G7 or E6 cells, constructs were induced with ponA (5 μM) and were visualized using eGFP (Ex 488 nm, Em 507 nm) or dsRed (Ex 558 nm, Em 583 nm) fluorescence using a confocal microscope (RS2; Leica, Heidelberg, Germany). Confocal analysis of in situ protein:protein association between eGFP-tagged RyR2 TM and coexpressed dsRed-tagged cytoplasmic domains was performed as described previously (George *et al.*, 2003a, 2003c).

Immunoprecipitation of RyR2 Domains

After induction with ponA (5 μM, 24 h), G7 and E6 cells expressing RyR2 N-terminal domains were homogenized in immunoprecipitation (IP) buffer (150 mM NaCl, 20 mM Tris, 2 mM DTT, 0.3% [wt/vol] CHAPS; pH 7.4) for 2 h at 4°C with constant orbital rotation. Samples were centrifuged (1500 × *g*, 10 min), and the supernatants were incubated with pAb129 (C-terminal) or pAb2143 (N-terminal; 1:200 dilution) for 36 h at 4°C. After incubation with protein G-agarose (20 μl; Santa Cruz Biotechnology; 1 h at 4°C) immunocomplexes were pelleted by centrifugation (2500 × *g*, 2 min), washed with IP buffer (3 × 1 ml) and immunoblotted using pAb129 or pAb2143 as described above.

[³H]Ryanodine Binding of RyR2 TM Domains

Microsomal fractions from G7 and E6 cells (uninduced or after incubation with ponA; 5 μM, 24 h) were obtained using an osmotic lysis procedure (George *et al.*, 2003c), and their specific ryanodine binding capacity was determined using a modification of a previous method (Holmberg and Williams, 1990). Briefly, membrane fractions were incubated with [³H]ryanodine (10 nM, Amersham) for 90 min at 37°C in a basic binding buffer (25 mM PIPES, 1 mM KCl; pH 7.4) containing ~100 μM free [Ca^{2+}]. Nonspecific binding was measured by coincubation with excess unlabeled ryanodine (10 μM). Bound [³H]ryanodine was separated from unbound using vacuum filtering through glass fiber filters (Whatman GF/F, Clifton, NJ) and filter-bound radioactivity was quantified by liquid scintillation counting. Microsomes obtained from cells expressing full-length RyR2 (George *et al.*, 2003b, 2003c) were used as controls.

Measurement of Intracellular [Ca^{2+}] and pH

In situ calibration of calcium crimson was performed in streptolysin O–permeabilized cells using buffers containing 0–39 μM free [Ca^{2+}] (George *et al.*, 2003b). Cells were loaded with calcium crimson (5 μM in Krebs-Ringer-HEPES (KRH) containing 1.3 mM $CaCl_2$ (KRH+Ca^{2+}; George *et al.*, 2003c) for 2 h at 30°C and transferred to KRH containing nominal free Ca^{2+} (KRH-Ca^{2+}, which contained 1 mM EGTA in place of 1.3 mM $CaCl_2$) immediately before experiments. Caffeine (10 mM) or 4-chloro-*m*-cresol (4-CMC, 1 mM) were used to trigger RyR-dependent intracellular Ca^{2+} release. In some experiments, cells were preincubated with ryanodine (1 mM) for 90 min and throughout the experiments and in others, cells were transfected with plasmid encoding human FKBP12.6 (George *et al.*, 2003c). To clamp intracellular [Ca^{2+}] in G7 and E6 cells, cells were incubated in solutions containing known free [Ca^{2+}] (approximately 150 nM and 300 nM, respectively) in the presence of ionomycin (1 μM, 30 min). Data were acquired from eGFP/dsRed-positive cells every 100 ms using a confocal microscope (RS2, Leica) and numerical data obtained from defined intracellular regions was converted to [Ca^{2+}] (George *et al.*, 2003b).

The intracellular pH of G7 or E6 cells expressing RyR2 N-termini was determined after the loading of BCECF-AM (2 μM, 45 min) and in situ calibration of H⁺-dependent BCECF fluorescence in KRH solutions at known

Figure 1. Schematic representation of truncated hRyR2 constructs. Putative TM regions (white bars) in RyR2^{4TM} and RyR2^{10TM} were reported previously (Takeshima *et al.,* 1989; Zorzato *et al.,* 1990). These constructs may also encode six TM-spanning regions (Du *et al.,* 2002; see MATERIALS AND METHODS). Domains A, B, and C represent putative functional regions within RyR2 predicted from primary sequence analysis and from data obtained elsewhere (Chen *et al.,* 1998; Du and MacLennan, 1999; Porter Moore *et al.,* 1999; Du *et al.,* 2000; Sun *et al.,* 2001). Dotted and striped bars represent eGFP and dsRed, respectively.
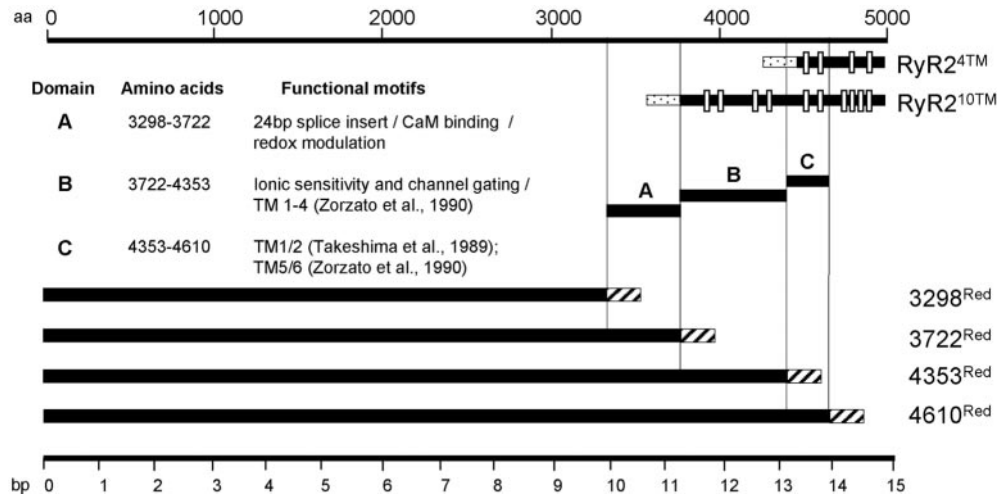
pH (pH 5.0–9.1) in the presence of nigericin (50 μM) and KCl (100 mM) using dual-wavelength excitation spectrophotometry (440 nm/490 nm; LS50B, Perkin Elmer-Cetus, Boston, MA). A pK_a of 7.132 (Hill slope = 0.559) was derived from nonlinear regression of the data using Prism software (GraphPad, San Diego, CA) and was used to obtain pH values from fluorescent data as described (Haugland, 1996).

Measurement of Fluorescence Resonance Energy Transfer

Fluorescence resonance energy transfer (FRET) between eGFP-tagged RyR2 TM domains and dsRed-tagged cytoplasmic domains was measured using the parameters described previously (Mizuno *et al.,* 2001). Briefly, induced G7 and E6 cells coexpressing cytoplasmic RyR2 domains were excited at 488 nm (Ex$_{max}$ eGFP) and fluorescent emission were monitored at 507 nm (Em$_{max}$ eGFP) and 583 nm (Em$_{max}$ dsRed). An increased Em 583:Em 507 ratio is a robust indicator of FRET occurring between eGFP and dsRed (Mizuno *et al.,* 2001). The FRET ratio (Em 583/507) was measured in single cells using a confocal microscope (Leica RS2) configured to ~4× oversampling (voxel size ~ 40 nm³) in identical experiments to those in which intracellular [Ca^{2+}] was determined. Numerical data was obtained from regions of interest focused to the immediate vicinity of membrane-associated eGFP-tagged RyR2 TM domains to minimize the contribution of cytoplasmic dsRed-tagged constructs occurring in the bulk cytoplasm to the FRET signal. Data were obtained from at least 60 cells using Leica software.

RESULTS

Characterization of the RyR2 TM Domain Using an Inducible Cell Model

cDNA constructs encoding the RyR2 TM and cytoplasmic domains used in this study are illustrated schematically in Figure 1. Cell lines G7 (RyR2^{4TM}) and E6 (RyR2^{10TM}) did not express detectable levels of recombinant RyR2 TM domains in the absence of ponA (Figure 2A). However, RyR2 TM domains of the predicted sizes (MW 85.6 and 170.9 kDa for eGFP-tagged RyR2^{4TM} and RyR2^{10TM}, respectively) were expressed in a dose-dependent manner after exposure of the cells to ponA (2–20 μM; Figure 2A). In situ detection of recombinant RyR2 TM domains in G7 and E6 cells using eGFP fluorescence confirmed a dose-dependent induction profile of RyR2^{4TM} and RyR2^{10TM}, respectively (Figure 2B). Increased expression levels of TM domains (>10 μM ponA) were associated with altered morphology (which was particularly pronounced in G7 cells), indicative of cellular toxicity (Figure 2B). Consequently, in subsequent experiments, ponA (5 μM) was used to induce sufficient TM domain expression to perform the experiments but which avoided the toxic effects associated with higher levels of RyR2 TM domain expression. RyR2^{4TM} and RyR2^{10TM} were detected
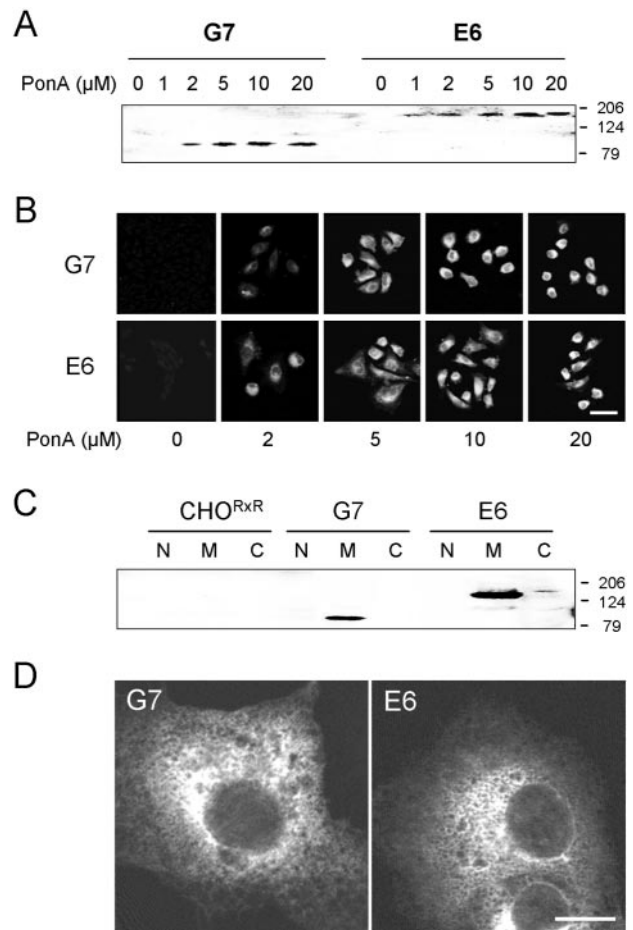

Figure 2. Heterologous expression of RyR2 TM domains in G7 and E6 cells. (A) Microsomal fractions (100 μg) obtained from G7 and E6 cells after ponA induction (0–20 μM) of RyR2^{4TM} and RyR2^{10TM}, respectively, were immunoblotted using pAb129. (B) Endogenous eGFP fluorescence was used to visualize RyR2^{4TM} and RyR2^{10TM} in G7 and E6 cells, respectively, after induction with ponA (0–20 μM). Bar, 10 μm. (C) Nuclear (N), microsomal (M), and cytosolic (C) fractions (100 μg) obtained from CHO^{RxR}, G7, and E6 cells exposed to ponA (5 μM) were immunoblotted using pAb129. (D) Intracellular localization of RyR2 TM domains in G7 and E6 cells after induction with ponA (5 μM). Bar, 5 μm.

only in microsomal fractions obtained from G7 and E6 cells, respectively (Figure 2C, lanes M) and not in nuclear or cytosolic fractions (lanes N and C, respectively). CHO^{RxR} did not express detectable levels of RyR in any subcellular fraction (Figure 2C). RyR2^{4TM} and RyR2^{10TM} in G7 and E6, respectively, exhibited endoplasmic reticulum (ER) localization characterized by a lattice-like distribution (Figure 2D).

After calibration of the Ca^{2+}-dependent fluorescence of calcium crimson in living cells ($K_{d(app)}$ = 493 nM, Hill Slope = 1.35), similar resting [Ca^{2+}]$_c$ in G7 (103 ± 9 nM) and E6 (92 ± 11 nM) cells were determined in the absence of ponA (Figure 3A, gray traces). After induction with a dose of ponA (5 μM), which induced expression of RyR2 TM domains but otherwise had little nonspecific effect on cell phenotype (Figure 2B), resting [Ca^{2+}]$_c$ was markedly elevated in G7 (279 ± 41 nM) and E6 (154 ± 23 nM) cells (Figure 3A, black traces) strongly indicating that RyR2 TM domains form Ca^{2+}-permeable conduits, entirely consistent with other studies (Bhat *et al.*, 1997; Xu *et al.*, 2000). Notably, similar expression levels of the RyR2 TM domains are achieved in G7 and E6 cells using this induction protocol (5 μM ponA, 24 h; Figure 2, A and B) and thus the different resting [Ca^{2+}]$_c$ measured in induced G7 and E6 cells was unlikely to be underscored by the differential expression of these Ca^{2+} permeable structures. Resting [Ca^{2+}]$_c$ in induced G7 or E6 cells was not altered after incubation with ryanodine, a specific modulator of intact RyR, or after coexpression of FKBP12.6, a potent modulator of full-length RyR2 Ca^{2+} release channels (George *et al.*, 2003b, 20023c; G7: 261 ± 37 and 308 ± 31 nM, respectively; E6: 162 ± 44 nM, 171 ± 29 nM, respectively; Figure 3B). Consistent with these results suggesting that the Ca^{2+}-releasing channels formed from RyR2^{4TM} and RyR2^{10TM} were refractory to modification by ryanodine in a cellular context, microsomal fractions obtained from induced G7 and E6 cells exhibited insignificant binding of [^{3}H]ryanodine (7.3 ± 5.9 and 5.2 ± 1.2 fmol/mg protein, respectively) when compared with microsomes containing comparable levels of full-length recombinant RyR2 (George *et al.*, 2003c; 82.6 ± 1.7 fmol/mg protein). Further, neither uninduced nor induced G7 and E6 cells (gray and black traces, respectively) were responsive to addition of caffeine (10 mM, arrowed), a potent RyR agonist, indicating that the Ca^{2+}-permeable structures formed by RyR2^{4TM} and RyR2^{10TM} were insensitive to caffeine activation (Figure 3C). Intracellular [Ca^{2+}] remained unchanged after addition of 4-CMC (1 mM) to induced G7 cells, but importantly, the addition of 4-CMC (1 mM) triggered a moderate but persistent increase in [Ca^{2+}]$_c$ in induced E6 cells only (186 ± 20 nM; Figure 3C, black traces). Uninduced G7 and E6 cell lines did not respond to 4-CMC (Figure 3D, gray traces), directly indicating that the [Ca^{2+}] increase in E6 cells after 4-CMC addition was indeed mediated by RyR2^{10TM}. This finding highlights that amino acid residues within RyR2^{10TM} confer sensitivity to activation by 4-CMC and is entirely consistent with the recent positional mapping of critical determinants of 4-CMC activation of RyR1 (Fessenden *et al.*, 2003). However, it should be noted that the magnitude of 4-CMC activation of Ca^{2+} release in E6 cells was markedly lower (~7%) than was measured in cells expressing full-length RyR2 after 4-CMC addition (753 ± 41 nM, where the percentage change in [Ca^{2+}] relative to resting [Ca^{2+}] was assigned 100%; Figure 3D). Also, caffeine (10 mM) elicited a large mobilization of Ca^{2+} through full-length recombinant RyR2, demonstrating that the agonist-response of full-length RyR2 in these cells remained intact (Figure 3D).
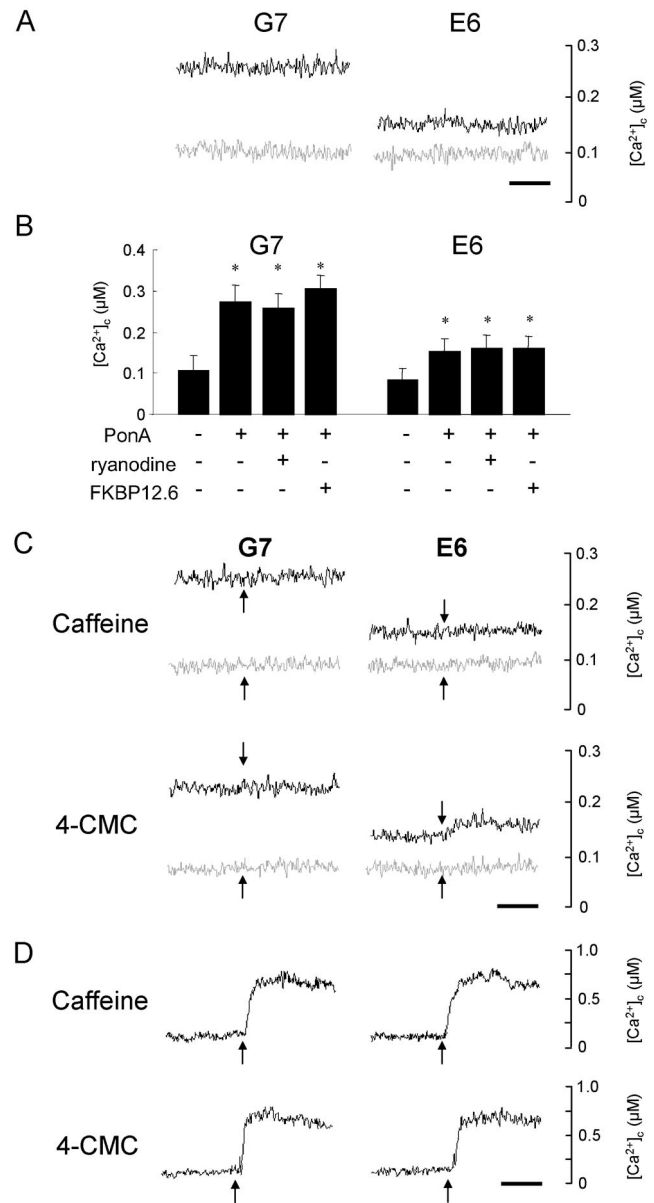

Figure 3. Intracellular Ca^{2+} handling in G7 and E6 cells. (A) Resting [Ca^{2+}]$_c$ was measured in uninduced G7 and E6 cells maintained in nominal free [Ca^{2+}] (gray traces) or after induction (ponA, 5 μM) of expression of RyR2^{4TM} and RyR2^{10TM}, respectively (black traces). (B) Resting [Ca^{2+}]$_c$ was measured in G7 and E6 cells or those pretreated with ryanodine or coexpressing FKBP12.6. The absence (−) or presence (+) of reagents is given. Data are plotted as means ± SEM (n = 5 with >30 cells analyzed in each instance). *p < 0.01. (C) The effect of caffeine (10 mM) or 4-CMC (1 mM) on intracellular Ca^{2+} release in uninduced (gray traces) or induced (black traces) G7 and E6 cells. Arrow indicates addition of agonist. (D) The effect of caffeine (10 mM) (C) or 4-CMC (1 mM) (D) on intracellular Ca^{2+} release in G7 and E6 cells expressing full-length RyR2. Arrow indicates agonist addition. Bar, 10 s.

Identification of an RyR2 Domain that Mediates N- and C-terminal Interaction

To determine the functional role of interdomain interaction on RyR Ca^{2+} release, we investigated the effects of coexpressing a panel of dsRed-tagged RyR2 amino-terminal domains on intracellular Ca^{2+} handling in G7 and E6 cells (see
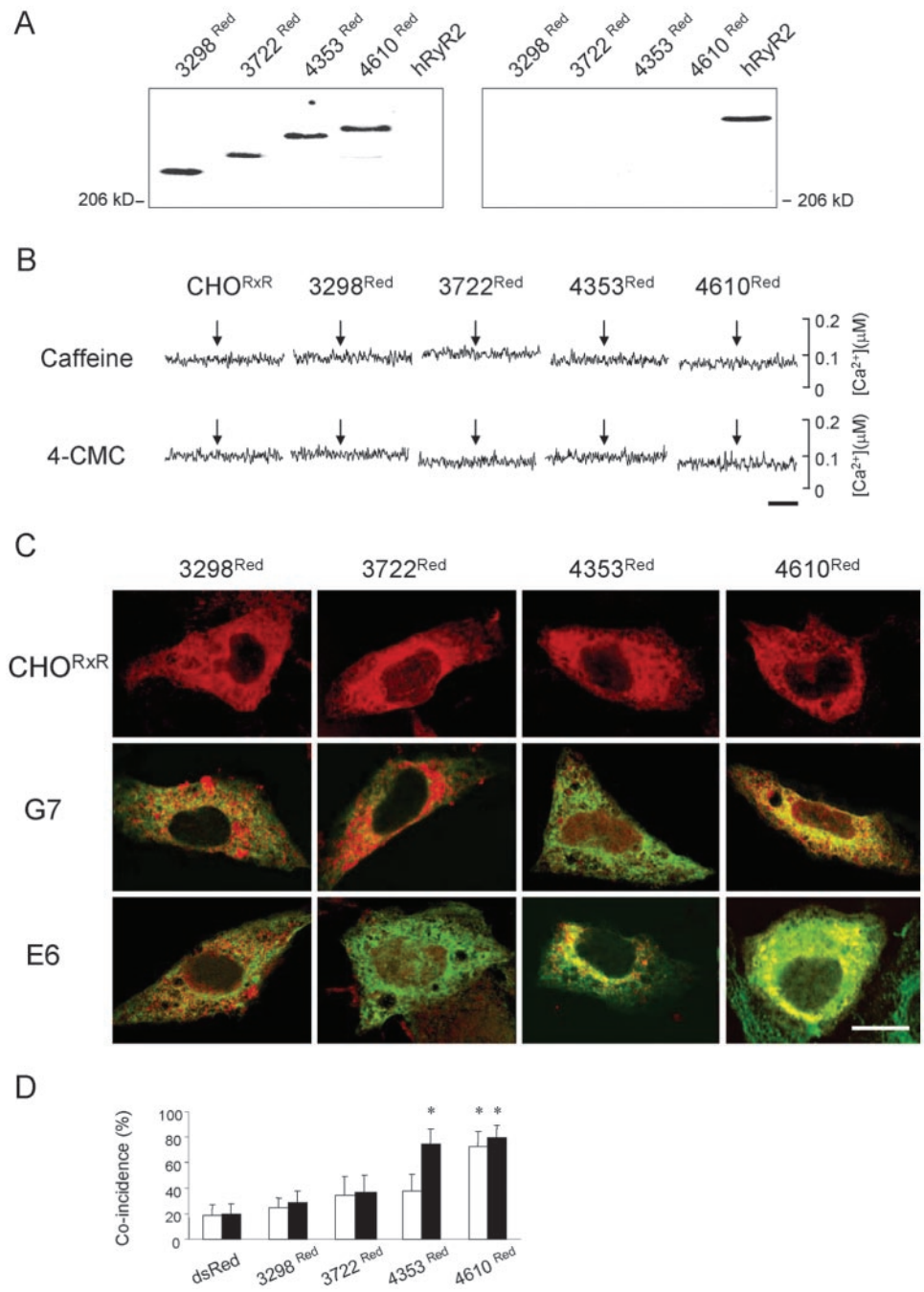
Figure 4. Characterization of recombinant RyR2 amino-terminal domains. (A) Cytoplasmic (left panel) and microsomal (right panel) fractions (100 μg) obtained from CHO^RxR cells expressing RyR2 N-terminal constructs were immunoblotted using pAb2143. Full-length recombinant RyR2 was used as control (MW ~565 kDa). (B) Intracellular Ca^2+ in CHO^RxR cells expressing RyR2 N-terminal domains was determined in resting cells and after the addition of caffeine (10 mM, top traces) and 4-CMC (1 mM, bottom traces; arrowed). Bar, 10 s. (C) The localization of RyR2 domains in CHO^RxR or G7 and E6 cells induced with ponA (5 μM) was determined using confocal microscopy. Coincidence of eGFP-tagged RyR2 TM domains (green) and dsRed tagged N-terminal domain (red) appears yellow. Bar, 10 μm. (D) Analysis of coincident staining between eGFP- and dsRed-tagged RyR2 constructs is expressed as the percentage of total cellular fluorescent signal of the RyR TM domains (green) that could be directly overlaid with fluorescence signal from dsRed tagged fusion proteins at 1024 × 1024 pixel resolution. G7 and E6 cells are represented as white and black bars, respectively. *p < 0.005 when compared with cells expressing untagged dsRed (n = 4, >12 cells per experiment).

Figure 1). Immunoblot analysis confirmed that recombinant proteins of the predicted molecular mass; 3298^Red (397.7 kDa) < 3722^Red (447.3 kDa) < 4353^Red (518.2 kDa) < 4610^Red (548.7 kDa) were expressed only in the cytoplasm of CHO^RxR (Figure 4A, left panel) and not in microsomal fractions (Figure 4A, right panel). In contrast, recombinant full-length RyR2 was abundant in microsomal preparations but totally absent in cytoplasmic fractions (Figure 4A, right and left panels, respectively), consistent with the identification of a membrane retention sequences in the extreme RyR carboxyl-terminus (Bhat and Ma, 2002). Expression of RyR2 N-terminal domains did not alter resting [Ca^2+] in CHO^RxR cells and did not confer agonist-sensitive Ca^2+ release after addition of caffeine or 4-CMC to cells (Figure 4B), strongly indicating that 3298^Red,

3722^Red, 4353^Red, and 4610^Red do not form Ca^2+-permeable structures in our cell system. Furthermore, these data suggest that RyR2 N-termini do not interact with other Ca^2+-releasing moieties in CHO^RxR cells because these cells remain refractory to RyR agonist-sensitive Ca^2+ release after their expression. In agreement with our subcellular fractionation data (Figure 2C), recombinant RyR2 N-terminal domains were characterized by homogeneous distribution throughout the cytoplasm in CHO^RxR cells (Figure 4C). Both 3298^Red and 3722^Red were abundantly expressed in the cytoplasm in induced G7 and E6 cells (Figure 4C, red), indicating minimal in situ association with either RyR2^4TM or RyR2^10TM. In contrast, there was a striking subcellular redistribution of 4353^Red toward intracellular membranes in induced E6 cells, but not in G7 cells (Figure
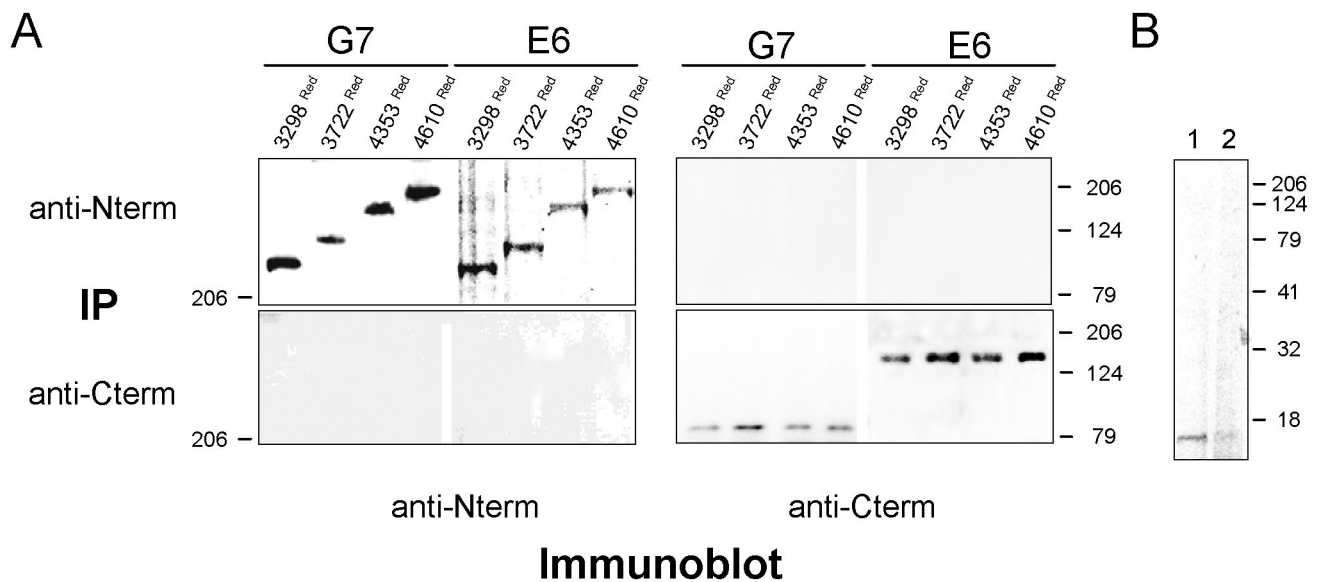
Figure 5. Interdomain association is mediated by weak protein:protein interaction. (A) Coimmunoprecipitation analysis of ponA induced (5 μM) G7 and E6 cells coexpressing 3298^{Red}, 3722^{Red}, 4353^{Red}, and 4610^{Red}. Postnuclear supernatants were immunoprecipitated using either pAb2143 (anti-N terminus) or pAb129 (anti-C terminus) and followed by immunoblotting using pAb2143 or pAb129 as described in MATERIALS AND METHODS. (B) Cell lysates (300 μg) from cells coexpressing recombinant FKBP12.6 and full-length RyR2 (George *et al.*, 2003c) were processed for immunoprecipitation using pAb129, and after separation using SDS-PAGE (20% acrylamide; vol/vol), FKBP12.6 was detected in the absence and presence of rapamycin (5 μM; lanes 1 and 2, respectively) using pAbN-19 (Santa Cruz Biotechnology).

4C). The majority of RyR2^{4TM} and RyR2^{10TM} in G7 and E6 cells, respectively, were colocalized with 4610^{Red} that exhibited extensive intracellular membrane localization (Figure 4C). Numerical analysis of pixel coincidence as a robust indicator of in situ protein:protein association (George *et al.*, 2003a, 2003c) demonstrated that sequence overlap between cytoplasmic and TM domains (broadly mapped to amino acids 3722–4610) promoted a marked sequestration of 4353^{Red} and 4610^{Red} to ER membranes containing RyR2 TM domains and provided good evidence of in situ association between RyR2 TM and cytoplasmic regions (Figure 4D). It should be noted that our analysis of RyR2 domain coincidence at high pixel resolution (1024 $\times$ 1024) specifically focused on the extent of association between ER membrane-localized TM domains with RyR2 N-terminal regions and thus represents a relative index of RyR2 N-terminal sequestration to ER membranes.

Using mild coimmunoprecipitation conditions (see MATERIALS AND METHODS) high-titer antipeptide antibodies raised against RyR2 carboxyl (pAb129) and amino-terminal (pAb2143) epitopes did not immunoprecipitate RyR2 cytoplasmic and TM domains, respectively, from postnuclear supernatants from transfected G7 and E6 cells, although these antibodies did immunoprecipitate the corresponding RyR2 domain (Figure 5A). Our coimmunoprecipitation methodology was validated by the coimmunoprecipitation of recombinant FKBP12.6 from cells which coexpressed full-length RyR2 (George *et al.*, 2003c; Figure 5B, lane 1), an interaction that could be disrupted by incubation of the cells with rapamycin (Figure 5B, lane 2). These results suggested that the association between RyR2 TM and cytoplasmic domains was mediated by weak protein:protein interactions.

RyR2 N- and C-terminal Interaction Critically Modulate Intracellular Ca^{2+} Handling

We next determined if the specific association between RyR2 TM and cytoplasmic domains, which was mediated by

amino acids 3722–4610, had a functional impact on the intracellular Ca^{2+} phenotype. We coupled determination of intracellular Ca^{2+} handling with FRET measurements between the eGFP and dsRed fusion partners (Mizuno *et al.*, 2001; Erickson *et al.*, 2003) to monitor in situ protein:protein association below the resolution limit of light microscopy (Day *et al.*, 2001; Kenworthy, 2001; Truong and Ikura, 2001). After expression of dsRed, resting [Ca^{2+}] remained unaltered and the lack of caffeine and 4-CMC sensitivity persisted when compared with non-dsRed–expressing induced G7 and E6 cells (Figure 6A, black traces, vs. Figure 3C). This data when taken together with the relatively low FRET signal determined in these cells ($\sim$ 0.6; Figure 6A, gray traces) indicated negligible interaction between dsRed and RyR2^{4TM} or RyR2^{10TM}. Coexpression of 3298^{Red} and 3722^{Red} in G7 and E6 cells did not affect resting [Ca^{2+}]$_c$, caffeine, or 4-CMC activation profiles (Figures 6, B and C, black traces, and 7), and FRET measurements were similar to those obtained in control cells expressing dsRed (Figures 6, B and C, gray traces, and 7), strongly suggesting that that 3298^{Red} and 3722^{Red} did not physically or functionally interact with RyR2^{4TM} or RyR2^{10TM}.

In marked contrast, 4353^{Red} demonstrated a dual mode of intracellular Ca^{2+} regulation in induced E6 cells, where its expression 1) significantly decreased resting [Ca^{2+}]$_c$ (Figures 6D, black trace, and 7A) and 2) restored caffeine-sensitive Ca^{2+} release to E6 cells expressing RyR2^{10TM} (Figures 6D, black trace, and 7B). These phenomena were associated with a significant increase in resting FRET ratio ($\sim$0.72) and caffeine-induced changes in the FRET signal (Figures 6D, gray trace, and 7, D and E), indicative of both increased steady-state interaction between 4353^{Red} and RyR2^{10TM} (Figure 7D) and caffeine-induced alterations in N- and C-terminal interaction (Figure 7E). This finding is in full agreement with our confocal analysis demonstrating in situ association between 4353^{Red} and RyR2^{10TM} (Figure 4, C and D), but
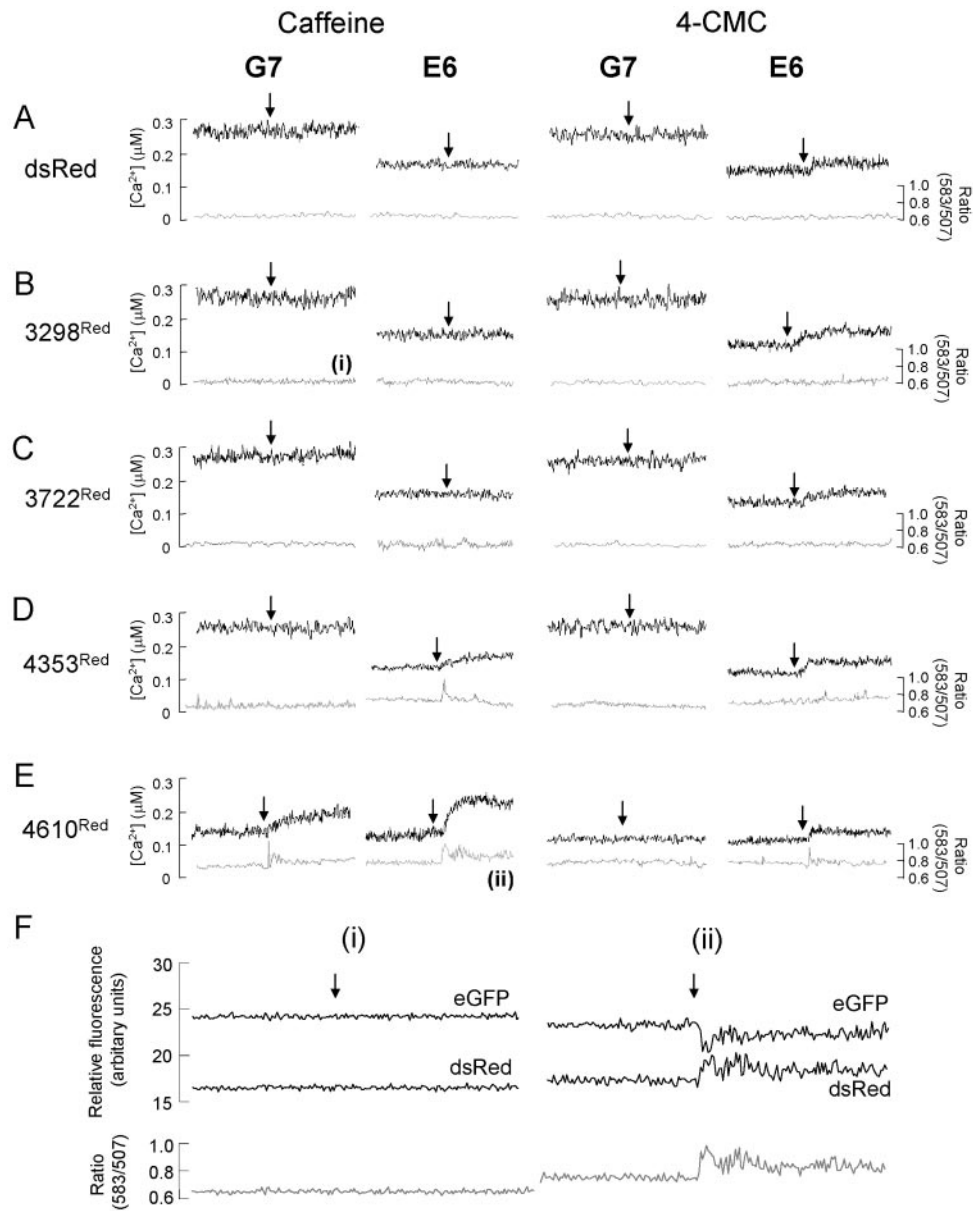
Figure 6. Investigating the functional impact of RyR2 TM and cytoplasmic domain interaction. (A–E) $[Ca^{2+}]_c$ in single G7 and E6 cells (black traces) coexpressing dsRed (A), 3298^{Red} (B), 3722^{Red} (C), 4353^{Red} (D), or 4610^{Red} (E) was measured before and after addition of caffeine or 4-CMC (arrowed). In parallel experiments, FRET (ratio 583:507; gray traces) between eGFP and dsRed fusion partners was determined. FRET ratio traces in B (i) and E (ii) are expanded in F. (F) Emission spectra (black traces) of eGFP (507 nm) and dsRed (583 nm) before and after addition of agonist (arrowed) used to derive the FRET ratio (gray traces) in B (i) and E (ii) are shown. Note that the caffeine-induced increase in FRET ratio in E6 cells expressing 4610^{Red} (F (ii)) is associated with decreased eGFP fluorescence and concomitantly increased dsRed fluorescence. Traces shown are representative of >30 imaged "positive" (eGFP and dsRed fluorescent) cells. Bar, 10 s.

significantly extends it further by revealing the functional impact of interdomain interaction on intracellular Ca^{2+} handling. Consistent with our data indicating that 4353^{Red} did not associate with $RyR2^{4TM}$ (Figure 4, C and D), expression of 4353^{Red} in G7 cells had little effect on resting $[Ca^{2+}]_c$ (Figures 6D, black trace, and 7A), agonist-induced Ca^{2+} release (Figure 6D, black traces and 7, B and C) and FRET ratio (Figures 6D, gray trace, and 7, D–F).

Importantly, upon extension of the RyR2 N-terminal domain to 4610 amino acids (i.e., incorporation of domain C, Figure 1), resting $[Ca^{2+}]_c$ was significantly decreased in both G7 and E6 cells coexpressing 4610^{Red} (Figures 6E, black

trace, and 7A) and was accompanied by an increased steady state resting FRET signal in these cells (~0.75; Figures 6E, gray trace, and 7D). Expression of 4610^{Red} further augmented caffeine-induced Ca^{2+} release in E6 cells when compared with expression of 4353^{Red}, and importantly 4610^{Red} also restored partial caffeine sensitivity in G7 cells (Figures 6E, black traces, and 7B). The 4610^{Red}-mediated restoration of caffeine sensitivity in both G7 and E6 cells was associated with increased peak FRET signal after caffeine addition (Figures 6E and 7E). Furthermore, the sustained elevation in $[Ca^{2+}]_c$ after the caffeine addition to E6 cells expressing 4610^{Red} was associated with a profound increase in ampli-
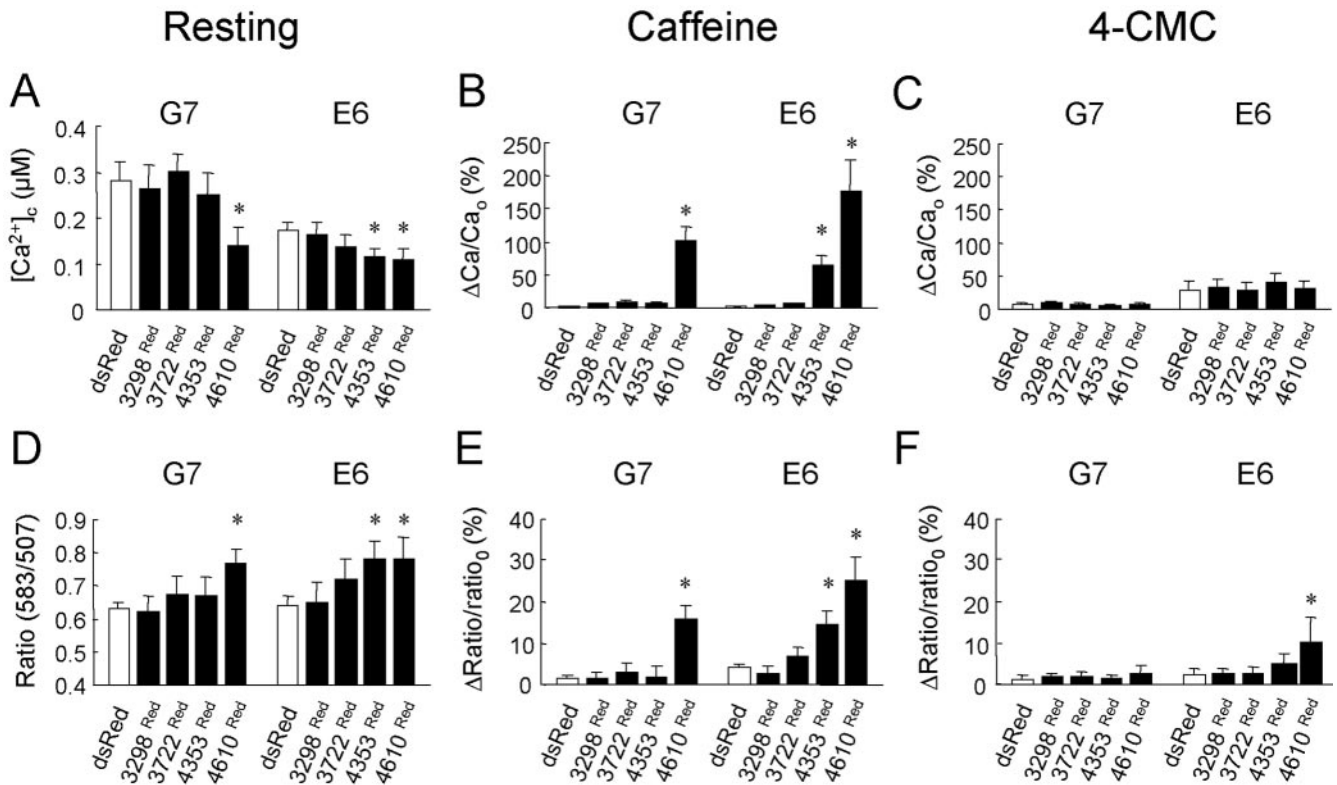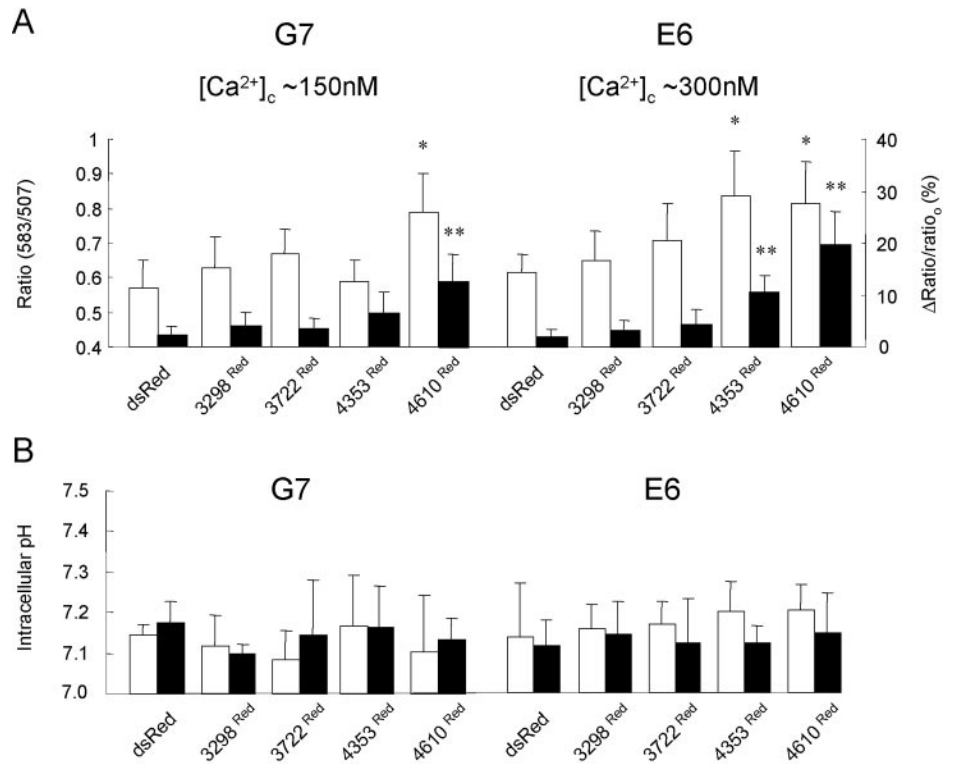
Figure 7. Interaction between RyR2 cytoplasmic and TM domains modulate intracellular Ca^{2+} in G7 and E6 cells. (A) Resting $[Ca^{2+}]_c$ measured in induced G7 and E6 cells transfected with dsRed, 3298^{Red}, 3722^{Red}, 4353^{Red}, and 4610^{Red}. (B and C) Increases in $[Ca^{2+}]_c$ after addition of caffeine (B) or 4-CMC (C) are represented as the percentage peak change in $[Ca^{2+}]_c$ (ΔCa) when compared with resting $[Ca^{2+}]_c$ (Ca_o). (D) Basal FRET signals (ratio 583:507) obtained from induced G7 and E6 cells expressing hRyR2 cytoplasmic domains. (E and F) Maximum agonist-induced changes in FRET signals after addition of caffeine (E) or 4-CMC (F) are expressed as the peak change in the FRET ratio (Δratio) when compared with the resting FRET ratio ($ratio_o$). All experimental values are plotted as means ± SEM (n > 30 cells) where the asterisk represents p <0.01 when compared with G7 or E6 cells expressing untagged dsRed.

tude variability in the FRET signal (Figure 6, E and F(ii)). This data raises the intriguing possibility that the increased "noise" in the FRET signal immediately after caffeine addition, which we logically interpret as agonist-induced conformational instability between RyR2 cytoplasmic and TM domains, may directly contribute to the sustained Ca^{2+} increase after caffeine activation of RyR2. The 4-CMC activation profile in G7 and E6 remained unchanged after the expression of all RyR2 cytoplasmic domains, suggesting that CMC activation of RyR2 is independent of interaction between cytoplasmic and TM domains (Figure 7C).

It was important to validate the FRET signals determined in these experiments, because FRET measurements may be critically influenced by the cellular environment including localized $[Ca^{2+}]$ and intracellular pH gradients. However, we have data strongly indicating that different intracellular Ca^{2+} environments in G7 and E6 cells did not contribute to the FRET measured between the eGFP and dsRed fusion partners in our experiments. First, the fluorescence emission spectra obtained from eGFP and dsRed are particularly diagnostic of bona fide FRET occurring because in cells where interaction occurs between RyR2 N-terminal and TM domains, there is decreased steady state eGFP emission accompanied by a corresponding increase in dsRed emission in resting cells, which is substantially augmented after caffeine addition (Figure 6F, trace (ii) compared with trace (i)). Second, using Ca^{2+} permeabilization techniques (see MATERIALS AND METHODS), the intracellular $[Ca^{2+}]$ in G7 and E6

cells were clamped at ~300 nM and ~150 nM, thereby reversing the resting intracellular Ca^{2+} environments normally found in these cells after induction of RyR2 TM domains (Figure 3C). Figure 8A shows that resting and caffeine-activated FRET signals after the switch in intracellular $[Ca^{2+}]$ in G7 and E6 cells expressing RyR2 N-terminal domains were similar to those data obtained in intact G7 and E6 cells (Figures 6 and 7). Thus, although the intracellular $[Ca^{2+}]$ in G7 and E6 cells was changed, the interactions of 4353^{Red} and 4610^{Red} with $RyR2^{4TM}$ and $RyR2^{10TM}$ in cells in which the $[Ca^{2+}]$ environment had been reversed (Figure 8A) were indistinguishable from the interactions determined in previous experiments (Figures 6 and 7). This finding strongly suggests that the different intracellular Ca^{2+} environments existing in induced G7 and E6 cells did not contribute to the FRET signals determined in this study. Third, intracellular pH in G7 and E6 cells expressing 3298^{Red}, 3722^{Red}, 4353^{Red}, or 4610^{Red} were similar in resting and caffeine-stimulated cells (Figure 8B), further reinforcing that although pH changes can affect FRET signals, differences in intracellular pH were unlikely to contribute to the differences in FRET signals determined in G7 and E6 cells. Thus, we interpret the increased resting FRET signals in E6 cells expressing 4353^{Red} and 4610^{Red} or G7 cells expressing 4610^{Red} (Figure 7D) as being due to increased proximity between the eGFP and dsRed FRET partners due to association between the N-terminal and TM domains of RyR2 and that the significantly increased FRET ratio after caffeine ad-

Figure 8. Investigating the impact of intracellular Ca^{2+} and pH environments on FRET between RyR2 cytoplasmic and TM domains. (A) The resting FRET ratio (ratio 583/507; white bars) or caffeine-induced changes in the FRET ratio ($\Delta ratio/ratio_o$; see Figure 7E legend; black bars) were determined in G7 and E6 cells, where intracellular $[Ca^{2+}]$ was clamped at approximately 150 and 300 nM, respectively, as described in MATERIALS AND METHODS. *p < 0.01 when the resting FRET signal is compared with G7 or E6 cells expressing dsRed, and **p < 0.01 when $\Delta ratio/ratio_o$ is compared with that measured in G7 or E6 cells expressing dsRed. n = 3 with >15 cells analyzed in each experiment. The data obtained from G7 and E6 cells expressing 3298^{Red} or 3722^{Red} did not attain significance (i.e., p > 0.05) in these experiments. (B) Intracellular pH in resting (white bars) and caffeine activated (10 mM; black bars) G7 and E6 cells expressing RyR2 N-terminal constructs was measured using BCECF (2 μM) after in situ calibration of the dye (see MATERIALS AND METHODS). n = 4 with >12 cells analyzed in each experiment.

dition is due to further rearrangement within the cytoplasmic and TM domain of RyR2 upon channel activation (Figures 6F and 7, E and F).

DISCUSSION

A novel in situ protein complementation approach was used to demonstrate that interaction between heterologously expressed RyR2 cytoplasmic and TM domains critically modulates intracellular Ca^{2+} handling and results in reconstitution of functional RyR2 channels. This finding provides the first cell-based insight into the precise mechanisms by which Ca^{2+} release channels autoregulate their activity via interdomain interaction. $RyR2^{4TM}$ and $RyR2^{10TM}$ were correctly targeted to the ER and formed Ca^{2+}-permeable conduits that exhibited different functional characteristics. $RyR2^{4TM}$ and $RyR2^{10TM}$ constructs were named according to the TM-spanning regions they were originally predicted to form (Takeshima et al., 1989; Zorzato et al., 1990), but more recently a 6TM model has been predicted (Du et al., 2002). Because it is highly unlikely that these constructs comprise different TM arrangements, we interpret our results to suggest that $RyR2^{4TM}$ and $RyR2^{10TM}$ form essentially the same Ca^{2+}-permeable structure but that $RyR2^{10TM}$ encodes additional modulatory regions (3722–4485 amino acids) that serve to regulate RyR2 Ca^{2+} release. This hypothesis is supported by the findings that the expression of $RyR2^{4TM}$ caused a dramatic elevation in cytoplasmic $[Ca^{2+}]$ in G7 cells, whereas cytoplasmic $[Ca^{2+}]$ was markedly lower in E6 cells expressing $RyR2^{10TM}$ despite equivalent levels of recombinant protein expression and that only $RyR2^{10TM}$ was sensitive to activation by 4-CMC. When taken together with theoretical and experimental modeling of the RyR C-terminus (Williams et al., 2001; Du et al., 2002), our results strongly suggest that the 3722–4485 amino acid region of RyR2 con-

tains modulatory domains that are involved in Ca^{2+} channel regulation. This is entirely consistent with our hypothesis that residues 3900–4500 do not form TM domains but that they represent regions of hydrophobicity (numerical index: +0.133; Hopp and Woods, 1981) critically involved in Ca^{2+} channel regulation. Furthermore, because the sequences encoding the 10TM model (Zorzato et al., 1990) are not present in $RyR2^{4TM}$, our results also provide good evidence that the C-terminus of RyR2 comprises an arrangement of four or six TM domains. $RyR2^{4TM}$ and $RyR2^{10TM}$ were refractory to modulation by ryanodine and FKBP12.6, emphasizing that the three-dimensional conformation of these binding sites requires the interaction of multiple domains in the intact RyR (Bultynck et al., 2001; Fessenden et al., 2001). In contrast to our findings, truncated RyR1 was modified by ryanodine (Bhat et al., 1997), but these constructs contained significant amino-terminal residues and thus the sole contribution of the Ca^{2+} pore-forming domain to ryanodine binding was not determined. Although the Ca^{2+}-forming pore of RyR2 was not modulated by coexpressed FKBP12.6, a potent regulator of full-length RyR2 (George et al., 2003c), we cannot exclude the possibility that the RyR2 TM domain bound FKBP12.6 but that there was insufficient RyR2 modulatory sequence present within these C-terminal domains to mediate FKBP12.6-dependent Ca^{2+} channel regulation.

Strikingly, we demonstrated a specific association between RyR2 cytoplasmic domains and the membrane localized TM region, which resulted in inhibitory (suppressed resting intracellular $[Ca^{2+}]$) and excitatory (restored caffeine sensitivity) modulation of RyR Ca^{2+} channel functionality. The marked functional interaction of RyR2 cytoplasmic and TM domains was mediated by weak physical interaction, which may reflect the dynamic mode of RyR regulation occurring in situ. By successive amino-terminal extension, the region mediating interaction between RyR2 TM and
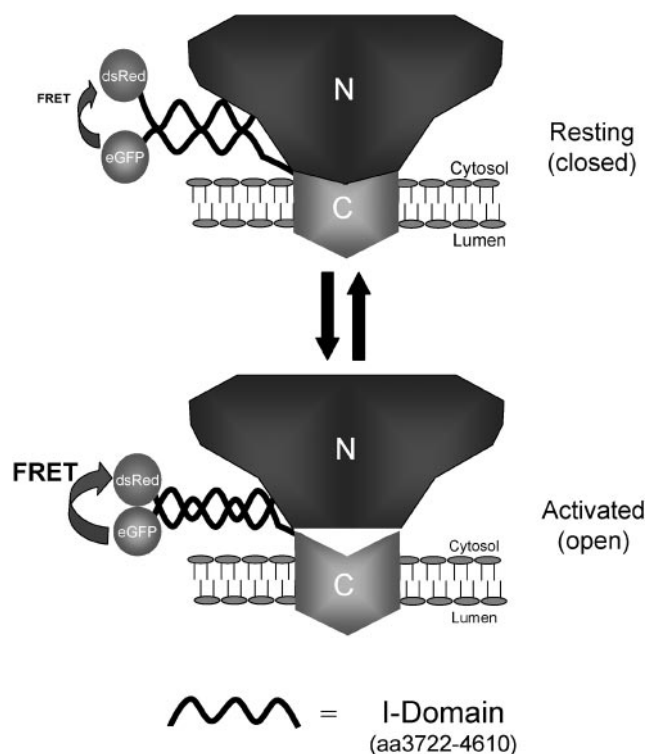
Figure 9. Schematic model of RyR regulation via interdomain interaction. A basal interaction between the cytoplasmic N-terminus of RyR2 and transmembrane C-terminus is mediated by amino acids 3722–4610 (I-domain) and suppresses aberrant Ca^{2+} release via the Ca^{2+}-channel pore. Caffeine activation triggers a conformational reorganization within the I-domain of the RyR polypeptide which results in increased FRET signal between dsRed and eGFP fusion partners (i.e., increased proximity of the fluorophores), and is associated with increased Ca^{2+} release through the RyR channel (see Figures 5 and 6).

cytoplasmic domains was mapped to amino-acid residues 3722–4610, which we termed the "interacting" or I-domain. Because the determinants of intersubunit interaction involved in RyR tetramerization are located in regions distinct from the I-domain (Stewart *et al.*, 2003), the I-domain probably mediates interaction within, and not between, RyR2 subunits in the intact tetramer. Because one RyR subunit contains a single I-domain, the interaction demonstrated in this study should be mediated by self-interaction *within* the I-domain of each RyR subunit. In support of this hypothesis, despite similar interaction with RyR2[10TM] in resting cells (Figure 7D), 4610[Red] significantly augmented caffeine-stimulated Ca^{2+} release when compared with these cells expressing 4353[Red] (Figure 7E). Thus, although amino acid residues 3722–4353 (Domain B, Figure 1) appear sufficient for interdomain interaction to occur with the RyR2[10TM] region, residues 4353–4610 (Domain C, Figure 1) markedly enhance the functional impact of this interaction. Therefore, our results indicate that interaction occurs between discrete regions of single I-domains, thereby resulting in the modulation of interaction between the cytoplasmic and TM assemblies of RyR2 (Figure 9), pointing to an additional complexity of interaction within the intact RyR that necessitates further experimentation. Although we provide strong evidence that the I-domain is essential for intraRyR interaction, we also cannot exclude the possibility that other cellular factors influence the association of RyR2 TM and N-terminal

domains and to this end, additional cellular factors affecting RyR interdomain interaction are currently being investigated. In a pathological context, the I-domain is the locus for several mutations associated with ventricular tachycardia (VT), where hyper-activation of the mutant RyR2 channel occurs after exposure to emotional or physical stress (Priori *et al.*, 2002) and it will be interesting to determine whether defective interaction of the I-domain within the intact RyR2 underlies the stress-induced VT phenotype. Clearly, a more precise analysis of the functional motifs involved in the intramolecular interaction which modulates RyR Ca^{2+} release remains to be determined.

The ability to investigate the dynamics of intracellular protein interaction below the limit of resolution of light microscopy is a major utility of FRET and the present study demonstrates the suitability of dsRed in partnering GFP in FRET studies. The use of dsRed as fusion partner has been restricted because of the slow maturation of the red fluorophore and its obligatory tetramerization (Baird *et al.*, 2000) but we did not encounter many of the reported difficulties of using dsRed, probably for the following reasons. First, our experimental protocol allowed sufficient time (~72 h) to maximize the maturation of the red fluorophore, resulting in negligible excitation of dsRed at the absorption maximum of GFP (488 nm). Second, the RyR fusion partners are sufficiently massive (>400 kDa) to negate the destabilizing effect of dsRed tetramerization on the correct folding of RyR2 domain structure. Third, the cytoplasmic domains of RyR are ordered in a loosely packed tetrameric arrangement within the native intact protein. Regarding these latter two points, although we currently do not know whether the dsRed-tagged RyR2 cytoplasmic domains adopt the complex structure determined in the intact RyR (Sharma *et al.*, 2000), our results clearly show that the folded state of these domains is both sufficient and necessary to modulate Ca^{2+} release via the pore-forming domain in our experimental system. However, it is acknowledged that potential problems may exist in using "tetrameric" dsRed as a fusion partner in other systems and to this end, the development of fluorescent dsRed monomers represents a significant advance in its use as a fusion partner (Campbell *et al.*, 2002).

An important finding of the present work is that caffeine activation of the channel required the transduction of modulatory events between the interacting cytoplasmic and TM domains of RyR and was associated with rearrangement within the protein:protein complex (Figure 9). This finding is entirely consistent with the long-range conformational changes associated with channel activation (Orlova *et al.*, 1996). Also, our results are in agreement with the demonstration that interaction occurs within the intact RyR tetramer (Zorzato *et al.*, 1996; Yamamoto *et al.*, 2000; Yamamoto and Ikemoto, 2002) but extend them further by showing that intraRyR interaction has a profound impact on RyR channel function and intracellular Ca^{2+} handling in a live-cell context, emphasizing the dynamic nature of intramolecular RyR interactions that may occur in vivo. Our findings may also represent a common regulatory mechanism of other Ca^{2+} release channels, notably the inositol 1,4,5-trisphosphate receptor (IP_3R), which also exhibits complex cytoplasmic architecture (Jiang *et al.*, 2002) and is also modulated by intramolecular interaction (Uchida *et al.*, 2003).

In summary, we propose a model of dynamic regulation of the Ca^{2+}-releasing pore of RyR2 by cytoplasmic domains in which intraRyR interaction is promoted by the specific association of hydrophobic domains. In a pathological context, defective regulation of RyR underlies aberrant Ca^{2+} release (George *et al.*, 2003a) and our cell-based model pro-

vides a powerful platform for a more detailed analysis of the specific role of RyR2 regulation by intramolecular interaction in disease phenotypes.

REFERENCES

Baird, G.S., Zacharias, D.A., and Tsien, R.Y. (2000). Biochemistry, mutagenesis, and oligomerisation of dsRed, a red fluorescent protein from coral. Proc. Natl. Acad. Sci. USA *97*, 11984–11989.

Balshaw, D., Gao, L., and Meissner, G. (1999). Luminal loop of the ryanodine receptor: a pore forming segment. Proc. Natl. Acad. Sci. USA *96*, 3345–3347.

Berridge, M.J., Lipp, P., and Bootman, M.D. (2000). The versatility and universality of calcium signalling. Nat. Rev. Mol. Cell. Biol. *1*, 11–21.

Bhat, M.B., and Ma, J. (2002). The transmembrane segment of ryanodine receptor contains an intracellular membrane retention signal for Ca^{2+} release channel. J. Biol. Chem. *277*, 8597–8601.

Bhat, M.B., Zhao, J., Takeshima, H., and Ma, J. (1997). Functional calcium release channel formed by the carboxyl-terminal portion of ryanodine receptor. Biophys. J. *73*, 1329–1336.

Bultynck, G., De Smet, P., Rossi, D., Callewaert, G., Missiaen, L., Sorrentino, V., De Smedt, H., and Parys, J.B. (2001). Characterization and mapping of the 12kDa FK506-binding protein (FKBP12)-binding site on different isoforms of the ryanodine receptor and of the inositol 1,4,5-trisphosphate receptor. Biochem. J. *354*, 413–422.

Callaway, C. *et al.* (1994). Localisation of the high and low affinity [³H] ryanodine binding sites on the skeletal muscle Ca^{2+} release channel. J. Biol. Chem. *269*, 15876–15884.

Campbell, R.E., Tour, O., Palmer, A.E., Steinbach, P.A., Baird, G.S., Zacharias, D.A., and Tsien, R.Y. (2002). A monomeric red fluorescent protein. Proc. Natl. Acad. Sci. USA *99*, 7877–7882.

Carafoli, E. (2002). Calcium signaling: a tale for all seasons. Proc. Natl. Acad. Sci. USA *99*, 1115–1122.

Chen, S.R.W., Ebisawa, K., Li, X., and Zhang, L. (1998). Molecular identification of the ryanodine receptor Ca^{2+} sensor. J. Biol. Chem. *273*, 14675–14678.

Chen, S.R.W., Li, P., Zhao, M., Li, X., and Zhang, L. (2002). Role of the proposed pore-forming segment of the Ca^{2+} release channel (ryanodine receptor) in ryanodine interaction. Biophys. J. *82*, 2436–2447.

Day, R.N., Periasamy, A., and Schaufele, F. (2001). Fluorescence resonance energy transfer microscopy of localised protein interactions in the living cell nucleus. Comp. Methods Enzymol. *25*, 4–18.

Doyle, D.A., Cabral, J.M., Pfuetzner, R.A., Kuo, A., Guibis, J.M., Cohen, S.L., Chait, B.T., and MacKinnon, R. (1998). The structure of the potassium channel: molecular basis of K^+ conduction and selectivity. Science *280*, 69–77.

Du, G.G., Guo, X., Khanna, V.K., and MacLennan, D.H. (2001). Functional characterization of mutants in the predicted pore region of the rabbit cardiac muscle Ca^{2+} release channel (ryanodine receptor isoform 2). J. Biol. Chem. *276*, 31760–31771.

Du, G.G., Khanna, V.K., and MacLennan, D.H. (2000). Mutation of divergent region 1 alters caffeine and Ca^{2+} sensitivity of the skeletal muscle Ca^{2+} release channel (ryanodine receptor). J. Biol. Chem. *275*, 11778–11783.

Du, G.G., and MacLennan, D.H. (1999). Ca^{2+} inactivation sites are located in the COOH terminal quarter of recombinant rabbit skeletal muscle Ca^{2+} release channels (ryanodine receptors). J. Biol. Chem. *274*, 26120–26126.

Du, G.G., Sandhu, B., Khanna, V.K., Guo, X.H., and MacLennan, D.H. (2002). Topology of the Ca^{2+} release channel of skeletal muscle sarcoplasmic reticulum (RyR1). Proc. Natl. Acad. Sci. USA *99*, 16725–16730.

El-Hayek, R., Saiki, Y., Yamamoto, T., and Ikemoto, N. (1999). A postulated role of the near amino-terminal domain of the ryanodine receptor in the regulation of the sarcoplasmic reticulum Ca^{2+} channel. J. Biol. Chem. *274*, 33341–33347.

El-Hayek, R., Yano, M., and Ikemoto, N. (1995). A conformational change in the junctional foot protein is involved in the regulation of Ca^{2+} release from sarcoplasmic reticulum. J. Biol. Chem. *270*, 15634–15638.

Erickson, M.G., Moon, D.L., and Yue, D.T. (2003). DsRed as a potential FRET partner with CFP and GFP. Biophys. J. *85*, 599–611.

Eu, J.P., Sun, J., Xu, L., Stamler, J.S., and Meissner, G. (2000). The skeletal muscle calcium release channel: coupled O_2 sensor and NO signaling functions. Cell *102*, 499–509.

Fessenden, J.D., Chen, L., Wang, Y., Paolini, C., Franzini-Armstrong, C., Allen, P.D., and Pessah, I.N. (2001). Ryanodine receptor point mutation E4032A reveals an allosteric interaction with ryanodine. Proc. Natl. Acad. Sci. USA *98*, 2865–2870.

Fessenden, J.D., Perez, C.F., Goth, S., Pessah, I.N., and Allen, P.D. (2003). Identification of a key determinant of ryanodine receptor type 1 required for activation by 4-chloro-m-cresol. J. Biol. Chem. *278*, 28727–27735.

Fill, M., and Copello, J.A. (2002). Ryanodine receptor calcium release channels. Physiol. Rev. *82*, 893–922.

Gao, L., Balshaw, D., Xu, L., Tripathy, A., Xin, C., and Meissner, G. (2000). Evidence for a role of the lumenal M3–M4 loop in skeletal muscle Ca^{2+} release channel (ryanodine receptor) activity and conductance. Biophys. J. *79*, 828–840.

Gao, L., Tripathy, A., Lu, X., and Meissner, G. (1997). Evidence for a role of C-terminal amino acid residues in skeletal muscle Ca^{2+} release channel (ryanodine receptor) function. FEBS Lett. *412*, 223–226.

George, C.H., Higgs, G.V., and Lai, F.A. (2003a). Ryanodine receptor mutations associated with stress-induced ventricular tachycardia mediate increased calcium release in stimulated cardiomyocytes. Circ. Res. *93*, 531–540.

George, C.H., Higgs, G.V., Mackrill, J.J., and Lai, F.A. (2003b). Dysregulated ryanodine receptors mediate cellular toxicity: restoration of normal phenotype by FKBP12.6. J. Biol. Chem. *278*, 28856–28864.

George, C.H., Sorathia, R., Bertrand, B.M.A., and Lai, F.A. (2003c). In situ modulation of the human cardiac ryanodine receptor (hRyR2) by FKBP12.6. Biochem. J. *370*, 579–589.

Grunwald, R., and Meissner, G. (1995). Lumenal sites and C-terminus accessibility of the skeletal muscle calcium release channel (ryanodine receptor). J. Biol. Chem. *270*, 11338–11347.

Haugland, R.P. (1996). Handbook of fluorescent probes and research products. Eugene, OR, Molecular Probes, 9th Edition. 831–832.

Holmberg, S.R.M., and Williams, A.J. (1990). The cardiac sarcoplasmic reticulum calcium release channel—modulation of ryanodine binding and single channel activity. Biochem. Biophys. Acta *1022*, 187–193.

Hopp, T.R., and Woods, K.R. (1981). Prediction of protein antigenic determinants from amino-acid sequences. Proc. Natl. Acad. Sci USA *78*, 3824–3828.

Ikemoto, N., and Yamamoto, T. (2000). Postulated role of inter-domain interaction within the ryanodine receptor in Ca^{2+} channel regulation. Trends Cardiovasc. Med. *10*, 310–316.

Jiang, Q.X., Thrower, E.C., Chester, D.W., Ehrlich, B.E., and Sigworth, F.J. (2002). Three-dimensional structure of the type 1 inositol 1,4,5-trisphosphate receptor at 24Å resolution. EMBO J. *21*, 3575–3581.

Kenworthy, A.K. (2001). Imaging protein-protein interactions using fluorescence resonance energy transfer microscopy. Comp. Methods Enzymol. *24*, 289–296.

Marx, S.O., Reiken, S., Hisamatsu, Y., Jayaraman, T., Burkhoff, D., Rosemblit, N., and Marks, A.R. (2000). PKA phosphorylation dissociates FKBP12.6 from the calcium release channel (ryanodine receptor): defective regulation in failing hearts. Cell *101*, 365–376.

Matz, M.V., Fradkov, A.F., Labas, Y.A., Savitsky, A.P., Zaraisky, A.G., Markelov, M.L., and Lukyanov, S.A. (1999). Fluorescent proteins from nonbioluminescent Anthozoa species. Nat. Biotechnol. *17*, 969–973.

McCarthy, T.V., Quane, K.A., and Lynch, P.J. (2000). Ryanodine receptor mutations in malignant hyperthermia and central core disease. Hum. Mutat. *15*, 410–417.

Meissner, G. (1994). Ryanodine receptor/Ca^{2+} release channels and their regulation by endogenous effectors. Annu. Rev. Physiol. *56*, 485–508.

Mizuno, H., Sawano, A., Eli, P., Hama, H., and Miyawaki, A. (2001). Red fluorescent protein from *Discosoma* as a fusion tag and a partner for fluorescence resonance energy transfer. Biochemistry *40*, 2502–2510.

No, D., Yao, T.P., and Evans, R.M. (1996). Ecdysone-inducible gene expression in mammalian cells and transgenic mice. Proc. Natl. Acad. Sci. USA *93*, 3346–3351.

Orlova, E.V., Serysheva, I.I., van Heel, M., Hamilton, S.L., and Chiu, W. (1996). Two structural configurations of the skeletal muscle calcium release channel. Nat. Struct. Biol. *3*, 547–552.

Porter Moore, C., Zhang, J.Z., and Hamilton, S.L. (1999). A role for cysteine 3635 of RyR1 in redox modulation and calmodulin binding. J. Biol. Chem. *274*, 36831–36834.

Priori, S.G. *et al.* (2002). Clinical and molecular characterization of patients with catecholaminergic polymorphic ventricular tachycardia. Circulation *106,* 69–74.

Sharma, M.R., Jeyakumar, L.H., Fleischer, S., and Wagenknecht, T. (2000). Three dimensional structure of ryanodine receptor isoform three in two conformational states as visualised by cryo-electron microscopy. J. Biol. Chem. *275,* 9485–9491.

Stewart, R., Zissimopoulos, S., and Lai, F.A. (2003). Oligomerization of the cardiac ryanodine receptor C-terminal tail. Biochem. J. *376,* 795–799.

Sun, J., Xin, C., Stamler, J.S., and Meissner, G. (2001). Cysteine 3635 is responsible for skeletal muscle ryanodine receptor modulation by NO. Proc. Natl. Acad. Sci. USA *98,* 11158–11162.

Takeshima, H. *et al.* (1989). Primary structure and expression from complementary-DNA of skeletal-muscle ryanodine receptor. Nature *339,* 439–445.

Tinker, A., and Williams, A.J. (1995). Measuring the length of the pore of the sheep cardiac sarcoplasmic reticulum calcium release channel using related trimethylammonium ions as molecular calipers. Biophys. J. *68,* 111–120.

Truong, K., and Ikura, M. (2001). The use of FRET imaging microscopy to detect protein-protein interactions and protein conformational changes in vivo. Curr. Opin. Struct. Biol. *11,* 573–578.

Tunwell, R.E.A., Wickenden, C., Bertrand, B.M.A., Shevchenko, V.I., Walsh, M.B., Allen, P.D., and Lai, F.A. (1996). The human cardiac muscle ryanodine receptor-calcium release channel: identification, primary structure and topological analysis. Biochem. J. *318,* 477–487.

Uchida, K., Miyauchi, H., Furuichi, T., Michikawa, T., and Mikoshiba, K. (2003). Critical regions for activation gating of the inositol 1,4,5-trisphosphate receptor. J. Biol. Chem. *278,* 16551–16560.

Williams, A.J., West, D.J., and Sitsapesan, R. (2001). Light at the end of the tunnel: structures and mechanisms involved in ion translocation in ryanodine receptor channels. Quart. Rev. Biophys. *34,* 61–104.

Witcher, D.R., McPherson, P.S., Kahl, S.D., Lewis, T., Bentley, P., Mullinnix, M.J., Windass, J.D., and Campbell, K.P. (1994). Photoaffinity labeling of the ryanodine receptor/Ca^{2+} release channel with an azido derivative of ryanodine. J. Biol. Chem. *269,* 13076–13079.

Xu, X., Bhat, M.B., Nishi, M., Takeshima, H., and Ma, J. (2000). Molecular cloning of cDNA encoding a Drosophila ryanodine receptor and functional studies of the carboxyl terminal calcium release channel. Biophys. J. *78,* 1270–1281.

Yamamoto, T., and Ikemoto, N. (2002). Peptide probe study of the critical regulatory domain of the cardiac ryanodine receptor. Biochem. Biophys. Res. Commun. *291,* 1102–1108.

Yamamoto, T., El-Hayek, R., and Ikemoto, N. (2000). Postulated role of interdomain interaction within the ryanodine receptor in Ca^{2+} channel regulation. J. Biol. Chem. *275,* 11618–11625.

Yin, C.C., and Lai, F.A. (2000). Intrinsic lattice formation by the ryanodine receptor calcium release channel. Nat. Cell Biol. *2,* 669–671.

Zhao, M., Li, P., Li, X., Zhang, L., Winkfein, R.J., and Chen, S.R.W. (1999). Molecular identification of the ryanodine receptor pore-forming segment. J. Biol. Chem. *274,* 25971–25974.

Zorzato, F., Fujii, J., Otsu, K., Phillips, M., Green, N.M., Lai, F.A., Meissner, G., and MacLennan, D.H. (1990). Molecular cloning of cDNA encoding human and rabbit forms of the Ca^{2+} release channel (ryanodine receptor) of skeletal muscle sarcoplasmic reticulum. J. Biol. Chem. *265,* 2244–2256.

Zorzato, F., Menegazzi, P., Treves, S., and Ronjat, M. (1996). Role of malignant hyperthermia domain in the regulation of Ca^{2+} release channel (ryanodine receptor) of skeletal muscle sarcoplasmic reticulum. J. Biol. Chem. *271,* 22759–22763.